IEEE Access
Multidisciplinary | Rapid Review | Open Access Journal

Received January 6, 2020, accepted January 30, 2020, date of publication February 5, 2020, date of current version February 12, 2020.

Digital Object Identifier 10.1109/ACCESS.2020.2971721

Wind-Speed Estimation and Sensorless Control for SPMSG-Based WECS Using LMI-Based SMC

MUHAMMAD ARIF SHARAFAT ALI[1], KHAWAJA KHALID MEHMOOD[2], SHAZIA BALOCH[1], AND CHUL-HWAN KIM[1], (Senior Member, IEEE)

[1]Department of Electrical and Computer Engineering, Sungkyunkwan University, Suwon 440-746, South Korea
[2]U.S.-Pakistan Centre for Advanced Studies in Energy (USPCAS-E), National University of Sciences and Technology, Islamabad 44000, Pakistan

Corresponding author: Chul-Hwan Kim (chkim@skku.edu)

This work was supported by the National Research Foundation of Korea (NRF) Grant funded by the Korea Government (MSIP) under Grant 2018R1A2A1A05078680.

ABSTRACT To enhance system reliability and to reduce the cost and complexity, this paper presents an efficient wind-speed estimation method and a sensorless rotor-position/speed control method for a surface-mounted permanent-magnet synchronous generator (SPMSG)-based variable-speed direct-drive wind-energy conversion system (WECS). In this regard, sliding mode control (SMC) based on a linear matrix inequality (LMI) is proposed to estimate the rotor position of an SPMSG. This method depends on measured electrical quantities, such as stator voltages and estimated stator current error, to evaluate the back electromotive force components, which are used to estimate the rotor position. The rotor speed is assessed according to the rate of change of the estimated rotor position. The wind speed is estimated by estimating the backpropagation power flow according to the nonlinear dynamical power wind-speed characteristics of the wind turbine. In estimating the rotor position, the proposed LMI-based SMC design provides good steady-state and dynamic performances under all operating modes of the WECS. The proposed control schemes are validated by simulating a test system, i.e., a 250-kW SPMSG-based WECS, in MATLAB/Simulink. The results confirm the effectiveness and correctness of the designed control schemes in estimating and tracking the actual rotor position/speed and wind speed with trivial errors.

INDEX TERMS Back electromotive force (BEMF), linear matrix inequality (LMI), sensorless control, sliding mode control (SMC), surface-mounted permanent-magnet synchronous generator (SPMSG), wind-energy conversion system (WECS).

I. INTRODUCTION

To satisfy the growing demand for energy, the dependency on ecofriendly renewable energy sources is increasing remarkably [1]. Among such energy sources, wind energy has attracted considerable attention as a clean and cost-effective source for electrical power production [2]. Considering that wind energy is a potential candidate for satisfying future energy needs, there have been significant developments in wind turbine (WT) technology with regard to size, control, and reliability. The concepts of variable-speed WTs and direct-drive wind-energy conversion systems (WECSs) have attracted special attention [3] because of their several inherent advantages, such as their high power density, operational efficiency, and reliability. Recently, the variable-speed WT equipped with a direct-drive permanent-magnet synchronous generator (PMSG) has been a widely accepted solution for obtaining highly reliable and efficient power generation [4], achieving good grid compatibility and low costs [2], and having the capability to ride through grid voltage dips [5].

The driving force for a WT is the wind speed. To perform several tasks, such as controlling, monitoring, and protecting the WT system, knowledge of the wind speed is indispensable. Generally, the wind speed is measured using well-calibrated mechanical sensors, which are known as anemometers. The disadvantages of using an anemometer are as follows: 1) reduced overall system performance, as it cannot measure the exact wind speed; 2) high initial costs, high failure rate, and maintenance issues due to limited accessibility; 3) the requirement for precise mounting and proper wiring, as well as a high vulnerability to electromagnetic noise, which makes the system less reliability and more complex.

The associate editor coordinating the review of this manuscript and approving it for publication was Jinquan Xu.

Similarly, precise knowledge of the absolute rotor position is required for controlling the torque generated by a PMSG and may also be needed if an application requires motion information. To serve this purpose, standardized mechanical rotor-position/speed sensors are installed at the generator shaft. However, such installations have issues similar to those associated with wind-speed sensors, which were previously discussed. Under the aforementioned circumstances, it is essential to remove such mechanical installations. A prospective solution for addressing these issues is to employ sensorless position/speed-control schemes to ensure system reliability. Motivated by the foregoing background, the authors intend to propose simple, precise, reliable, economical, and widely applicable solutions for wind-speed estimation and sensorless rotor position/speed control for a PMSG in a wind-power system (WPS) and to assess the functionalities of the proposed schemes over the full operational regimes of a WECS.

Extensive efforts have been directed toward developing sensorless control methods for WECSs for estimating wind speed [5]–[16]. In [6], the authors proposed an artificial neural network to estimate the wind speed. A power signal feedback method was adopted in [7] to predict the wind speed. An autoregressive statistical model was utilized to estimate the wind speed in [8]. The authors of [9] proposed a wind-speed estimation method based on support vector regression. An extreme learning machine-based wind-speed estimator was presented in [10]. In [11], the authors developed a nonlinear estimator for wind-speed measurement using a Kalman filter. The wind speed was calculated by estimating the aerodynamic torque, rotor speed, and pitch angle, in [12]. A frequency-domain fusion technique was proposed for predicting the effective wind speed in [13]. The authors of [14], [15] suggested adaptive neuro-fuzzy inference systems for estimating the wind profile. In [16], wind-speed prediction was performed using a maximum likelihood estimator.

Extensive literature is available for rotor-position/speed estimation techniques, ranging from open-loop to modern closed-loop observers. Owing to their good disturbance rejection and robustness to the system parameters, closed-loop observers—including disturbance observers, sliding-mode observers (SMOs), model reference adaptive system (MRAS)-based observers, and back electromotive force (BEMF)-based phase-locked loop (PLL) observers—have attracted increasing attention. A disturbance observer-based EMF was proposed in [17], [18]. SMOs are very effective for estimating the rotor position/speed, as the dynamics for the states of interest depend only on the manifold chosen and are not affected by the system's parameters [19]. In [20], the robustness of the rotor-speed estimation was improved using an online SMO adaption scheme. An extended EMF model-based SMO was proposed in [21]. BEMF-based PLLs have been widely investigated for sensorless control of PMSGs [4], [22]–[24]. In [4], a finite control set based on model predictive control was suggested for estimating the BEMF, which was then used to estimate the rotor position. An SMO in combination with a PLL was used in [22] to enhance the position-estimation performance. In [23], the authors presented an adaptive neural-network-based filter to alleviate the harmonic ripple in the BEMF. A combination of a PLL and high-frequency injection was employed to determine the rotor position in [24]. MRAS-based methods are very effective for speed estimation [5], [25]–[27]. References [5] and [25] proposed BEMF-based MRAS observers for estimating the shaft speed, whereas an MRAS based on control of the winding-current error was suggested in [26]. In [27], the authors presented an MRAS based on active power for speed estimation of a doubly fed reluctance generator. Other methods have also been proposed [28]–[31]. In [28], the rectifier voltage ripples were utilized to achieve sensorless control of a generator, and the direct-current (DC) magnitude of the rectifier output was used in [29]–[31] for the same purpose.

Enhancing the system reliability and reducing the complexity and cost were the ultimate objectives of this study; these were achieved by 1) developing an efficient scheme for wind-speed estimation without a measuring device and 2) developing a sensorless control scheme for a surface-mounted PMSG (SPMSG) incorporated into a direct-drive variable-speed WECS, in which no rotor-position/speed sensors are needed. This study was performed as follows:

- First, a sliding mode control (SMC) method based on a linear matrix inequality (LMI) is proposed and is developed with an adjustable SPMSG model for rotor-position estimation to efficiently track the actual position.
- Second, the rotor speed is estimated according to the rate of change of the estimated rotor position. A low-pass filter is employed to filter the speed signal and to remove the high-frequency noise.
- Third, wind-speed estimation is realized according to the power flow in a WECS, and the kinetic energy (*KE*) of the incoming wind is estimated in the backpropagation mode.
- Detailed theoretical derivations and approaches are discussed to verify the stability and validity of the proposed control schemes.
- Finally, the wind speed is determined via the available estimations of the wind power and rotor speed. The wind speed is then used to generate the speed reference for controlling the SPMSG.

The contributions of the study are summarized as follows:

1) A simple wind-speed estimation method based on the estimated power flow in the system was developed and evaluated.
2) An SMC method based on an LMI was proposed for estimating the rotor position. It can track the actual rotor position precisely, with trivial errors.
3) Simple, efficient, and cost-effective solutions were provided for controlling the direct-drive SPMSG-based WECS and eliminating the sensor requirements for

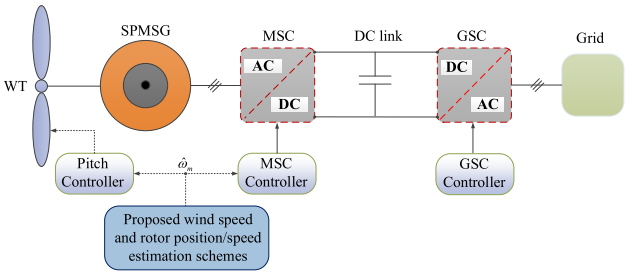

FIGURE 1. Configuration of a direct-drive SPMSG-based WECS.

measuring the wind speed, rotor position, and rotor speed, thereby enhancing the system reliability and reducing the complexity.

The remainder of this paper is organized as follows. The grid-connected WECS is briefly described in Section II. Detailed design procedures for wind-speed estimation and sensorless control for an SPMSG using LMI-based SMC method are presented in Section III. The closed-system stability analysis is illustrated in Section IV. The mathematical modeling and formulation of the full-scale converters (FSCs) are explained in Section V. In Section VI, numerical simulation results for a test system are presented and discussed after the proposed estimation schemes are applied. Concluding remarks are presented in Section VII.

II. DESCRIPTION OF GRID-CONNECTED DIRECT-DRIVE WECS

A typical configuration of a wind-power-generation system is illustrated in Fig. 1. The system consists of a direct-drive WT, an SPMSG, and FSCs. FSCs are generally adopted to serve as an interface between the WECS and the power grid, to control the SPMSG and regulate the frequency and voltage of generated electricity, which is necessary for fulfilling the grid code requirements. An FSC system comprises a machine-side converter (MSC), a DC-link, a grid-side converter (GSC), and an associated control system. The output of the FSC is rectified by the MSC and then supported by the DC-link, and finally, the power is transferred to the grid through the GSC. The control objective of the MSC is to regulate the SPMSG output power with a variable frequency and voltage into DC power, whereas the DC-link voltage regulation and the exchange of reactive power between the FSC and the grid are achieved by the GSC. Extensive formulation, implementation, and analyses of the proposed estimation schemes are presented in Section III.

III. PROPOSED CONTROL SCHEMES

This section addresses the theoretical concepts, mathematical modeling, detailed design methodologies, and analyses of the proposed control schemes for wind-speed and rotor-position/speed estimations, thus making the sensorless control for an SPMSG possible in a WPS.

A. WIND-SPEED ESTIMATION

In this study, a simple wind-speed estimation method based on the nonlinear dynamical power wind-speed characteristics

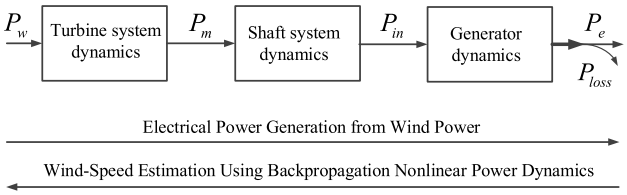

FIGURE 2. Power flow of the WT generation system for wind-speed estimation.

of a WT is developed. This method uses the estimated system power in the backpropagation manner. The *KE* of the incoming wind depends on the wind speed only, and this relationship is used to estimate the wind speed. The process of converting the *KE* of the incoming wind into electrical power in a WT generation system is shown in Fig. 2. The procedure for estimating the wind speed is shown in Fig. 2.

A PMSG is modeled in a *dq* synchronously rotating frame (SRF). For an SPMSG, the *d*-axis and *q*-axis have the same inductance. Therefore, it is assumed that $L_d = L_q = L_s$. The generator output power is calculated as follows:

$$P_e = v_a i_a + v_b i_b + v_c i_c \tag{1}$$

In (1), *v* and *i* represent the voltage and current quantities, respectively. The power losses of an SPMSG involve four components (2): 1) copper losses in the stator windings, 2) mechanical losses, 3) core losses, and 4) stray losses.

$$P_{losses} = P_{cu-loss} + P_{mech-loss} + P_{core-loss} + P_{stray-loss} \tag{2}$$

The copper losses in the stator windings can be calculated as follows:

$$P_{cu-loss} = 1.5\left(i_{ds}^2 + i_{qs}^2\right) R_s = 1.5 i_s^2 R_s. \tag{3}$$

Here, the subscript *s* denotes the stator-side quantities; the subscripts *d* and *q* represent the *d*- and *q*-axis components of the quantities in the SRF; *R* is the resistance. The mechanical losses, which are also known as rotational losses, are frequently lumped with core losses and depend on the rotating speed and flux linkage [5]. The core and friction losses together are assumed to be 1% of the generator rated power [32]. The stray losses are assumed to be 1% of the generator electrical power [33]. Utilizing the measured generator output power (1) and the estimated value of the power losses (2), the input power to the SPMSG can be approximated as follows:

$$\hat{P}_{in} = P_e + \hat{P}_{losses}, \tag{4}$$

In (4), the symbol ^denotes estimated values. As previously discussed, the WT is directly connected to the SPMSG; therefore, the shaft system can be represented by a one-mass model, whose dynamics are given by a differential equation:

$$\left.\begin{aligned} J\frac{d}{dt}\omega_m &= T_m - T_e - D\omega_m \\ J\frac{d}{dt}\omega_m &= \frac{P_m}{\omega_m} - \frac{P_e}{\omega_m} - D\omega_m \end{aligned}\right\}, \tag{5}$$

Here, J represents the combined inertia of the turbine and generator; D is the viscous damping coefficient; ω_m being the mechanical rotor speed. The turbine mechanical power (P_m) can be estimated using (5) and is given as

$$\hat{P}_m = \hat{\omega}_m(t) J \frac{d}{dt}\hat{\omega}_m + \hat{P}_{in}(t) + D\hat{\omega}_m^2. \tag{6}$$

From (6), it is clear that the turbine power can be estimated by knowing the turbine shaft speed in advance. The process of estimating the rotor speed is described in detail in the next subsection. The *KE* of the incoming wind can be approximated as follows:

$$\hat{P}_w(t) = \frac{\hat{P}_m(t)}{\hat{C}_P(\lambda, \beta)}, \tag{7}$$

In (7), C_P is the performance coefficient of the WT, λ represents the tip-speed ratio of the WT, which defines the relationship between the wind speed and rotor speed [34], and β represents the pitch angle. Finally, the wind speed can be estimated as follows, assuming that the air density (σ) is constant:

$$\hat{v}_w(t) = \left[\frac{\hat{P}_w(t)}{K_P}\right]^{\frac{1}{3}}, \quad K_P = 0.5\rho A_{WT}, \tag{8}$$

Here, A_{WT} represents the area of the WT rotor.

B. ESTIMATION OF ROTOR POSITION AND SPEED

The phase voltage of an SPMSG, which depends on the generator speed, can be expressed as follows [35]:

$$V = E - I\left(R_s + j\omega_e L_s\right), \tag{9}$$

Here, L represents the inductance, whereas E represents the BEMF of the generator and is proportional to the generator speed (ω_e).

$$E = K_w \omega_e \tag{10}$$

Here, K_w is the coefficient between the BEMF and the generator speed, and it represents the flux linkage of the permanent magnets. Sensorless control for an SPMSG is achieved by transforming its model into a stationary reference frame. Clark transformation is employed to convert the stator voltage from the *abc* frame to the $\alpha\beta$ frame, as follows:

$$\begin{bmatrix} v_{\alpha s} \\ v_{\beta s} \end{bmatrix} = \begin{bmatrix} 1 & -\frac{1}{2} & -\frac{1}{2} \\ 0 & \frac{\sqrt{3}}{2} & -\frac{\sqrt{3}}{2} \end{bmatrix} \begin{bmatrix} v_{as} \\ v_{bs} \\ v_{cs} \end{bmatrix}. \tag{11}$$

The dynamical model for the SPMSG is obtained in the stationary $\alpha\beta$ reference frame and is expressed as

$$\begin{bmatrix} v_{\alpha s} \\ v_{\beta s} \end{bmatrix} = \left(R_s + \frac{d}{dt}L_s\right) \begin{bmatrix} i_{\alpha s} \\ i_{\beta s} \end{bmatrix} + \omega_e \psi_{PM} \begin{bmatrix} -\sin\theta_m \\ \cos\theta_m \end{bmatrix}, \tag{12}$$

In (12), ψ_{PM} represents the flux linkage generated by the permanent magnets. Estimating the rotor position using (12), it is assumed that the stator voltage, stator current, and machine parameters are known. Equation (12) can also be expressed as follows:

$$\begin{bmatrix} v_{\alpha s} \\ v_{\beta s} \end{bmatrix} = \begin{bmatrix} R_s & 0 \\ 0 & R_s \end{bmatrix} \begin{bmatrix} i_{\alpha s} \\ i_{\beta s} \end{bmatrix} + \frac{d}{dt} \begin{bmatrix} L_s & 0 \\ 0 & L_s \end{bmatrix} \begin{bmatrix} i_{\alpha s} \\ i_{\beta s} \end{bmatrix} + \begin{bmatrix} e_{\alpha s} \\ e_{\beta s} \end{bmatrix}. \tag{13}$$

In this study, an LMI-based SMC method is designed to track the actual rotor position of an SPMSG. Consideration of the equations that describe the electromagnetic behavior of the machine is the starting point for LMI-based SMC design. The state-space model of an SPMSG in the matrix form is expressed as follows:

$$\begin{aligned} \frac{d}{dt}\begin{bmatrix} i_{\alpha s} \\ i_{\beta s} \end{bmatrix} &= \begin{bmatrix} -\frac{R_s}{L_s} & 0 \\ 0 & -\frac{R_s}{L_s} \end{bmatrix} \begin{bmatrix} i_{\alpha s} \\ i_{\beta s} \end{bmatrix} + \begin{bmatrix} \frac{1}{L_s} & 0 \\ 0 & \frac{1}{L_s} \end{bmatrix} \begin{bmatrix} v_{\alpha s} \\ v_{\beta s} \end{bmatrix} \\ &\quad - \begin{bmatrix} \frac{1}{L_s} & 0 \\ 0 & \frac{1}{L_s} \end{bmatrix} \begin{bmatrix} e_{\alpha s} \\ e_{\beta s} \end{bmatrix} \\ \left[\dot{i}_s\right] &= A\left[i_s\right] + B\left[v_s - e_s\right], \end{aligned} \tag{14}$$

Here, the matrices A and B and the stator current, stator voltage, and BEMF vectors are expressed as follows:

$$A = \begin{pmatrix} -\frac{R_s}{L_s} & 0 \\ 0 & -\frac{R_s}{L_s} \end{pmatrix}, \quad B = \begin{pmatrix} \frac{1}{L_s} & 0 \\ 0 & \frac{1}{L_s} \end{pmatrix}$$

$$i_s = \begin{pmatrix} i_\alpha & i_\beta \end{pmatrix}^T, \quad v_s = \begin{pmatrix} v_\alpha & v_\beta \end{pmatrix}^T, \quad e_s = \begin{pmatrix} e_\alpha & e_\beta \end{pmatrix}^T$$

The values of the rotor angular position (θ_e) and rotor speed (ω_e) are unknown. Thus, it is unavoidable to design a dynamic system that has a structure resembling (14) and uses the same available information about the stator voltage and current (15).

$$\begin{aligned} \frac{d}{dt}\begin{bmatrix} \hat{i}_{\alpha s} \\ \hat{i}_{\beta s} \end{bmatrix} &= \begin{bmatrix} -\frac{R_s}{L_s} & 0 \\ 0 & -\frac{R_s}{L_s} \end{bmatrix} \begin{bmatrix} \hat{i}_{\alpha s} \\ \hat{i}_{\beta s} \end{bmatrix} \\ &\quad + \begin{bmatrix} \frac{1}{L_s} & 0 \\ 0 & \frac{1}{L_s} \end{bmatrix} \left(\begin{bmatrix} v_{\alpha s} \\ v_{\beta s} \end{bmatrix} - \begin{bmatrix} \hat{e}_{\alpha s} \\ \hat{e}_{\beta s} \end{bmatrix} \right) \\ \left[\dot{\hat{i}}_s\right] &= A\left[\hat{i}_s\right] + B\left[v_s - \hat{e}_s\right] \end{aligned} \tag{15}$$

To reflect the processes correctly, systems (14) and (15) must coincide. The control goal is

$$\hat{i}_s \to i_s. \tag{16}$$

The tracking error is defined as

$$z = \hat{i}_s - i_s. \tag{17}$$

Then,

$$\dot{z} = \dot{\hat{i}}_s - \dot{i}_s = A\hat{i}_s + Bu - \dot{i}_s. \tag{18}$$

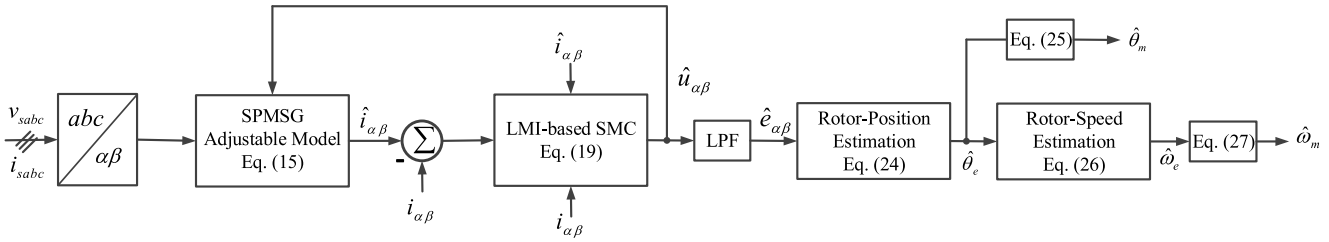

FIGURE 3. Schematic of the LMI-based SMC method for SPMSG rotor-position/speed estimations.

A controller is designed as follows:

$$u = G\hat{i}_s + u_r, \tag{19}$$

In (19), G represents the state feedback gain matrix, which can be obtained using the LMI, and u_r is given as

$$u_r = -Gi_s - B^{-1}Ai_s + B^{-1}\dot{i}_s. \tag{20}$$

Then,

$$\left.\begin{aligned} u &= G\hat{i}_s - Gi_s - B^{-1}Ai_s + B^{-1}\dot{i}_s \\ u &= Gz - B^{-1}Ai_s + B^{-1}\dot{i}_s \end{aligned}\right\} \tag{21}$$

and

$$\left.\begin{aligned} \dot{z} &= A\hat{i}_s + B\left(Gz - B^{-1}Ai_s + B^{-1}\dot{i}_s\right) - \dot{i}_s \\ &= A\hat{i}_s + BGz - Ai_s + \dot{i}_s - \dot{i}_s \\ &= Az + BGz \end{aligned}\right\}. \tag{22}$$

Theorem 1: If the following LMI is satisfied

$$\mu S + A^T S + Q^T + SA + Q < 0, \mu > 0, \tag{23}$$

where

$$G = (SB)^{-1} Q.$$

Then, according to (23), the closed system with the model (15) and controller (19) is exponentially stable. It is worthwhile to mention that there is no deviation between the estimated and actual rotor positions.

After obtaining the estimated values of the BEMF vector components, the rotor electrical and mechanical angles are estimated using (24) and (25), respectively:

$$\hat{\theta}_e = \tan^{-1}\left(\frac{\hat{u}_\beta}{\hat{u}_\alpha}\right) \tag{24}$$

$$\hat{\theta}_m = \frac{\hat{\theta}_e}{n_p}, \tag{25}$$

In (25), n_p represents the number of pole pairs. A schematic of the proposed LMI-based SMC method for sensorless control of a direct-drive SPMSG is presented in Fig. 3

The necessary information about the rotor speed is expressed as shown in (26), by the rate of change of the estimated rotor position.

$$\hat{\omega}_e = \frac{d\hat{\theta}_e}{dt} = \frac{\hat{\theta}_e(k) - \hat{\theta}_e(k-1)}{T_c} \tag{26}$$

Here, T_c represents the sampling period. The rotor mechanical speed is determined as follows:

$$\hat{\omega}_m = \frac{\hat{\omega}_e}{n_p}. \tag{27}$$

IV. CLOSED-SYSTEM STABILITY ANALYSIS

This section mainly focuses on describing the stability analysis of the closed system with the proposed controller. In this context, first, the Lyapunov stability is studied, which permits to develop the core of this section: the stability analysis of the closed system.

A. LYAPUNOV STABILITY

Consistent with the design of feedback SMC, the tracking error (17) converges to zero exponentially. The proof is made by 1) Lyapunov stability criterion is formulated concerning the solution of a matrix equation and 2) Lyapunov stability of the controller is presented.

Theorem 2: Consider the system $\dot{x} = Ax$ is exponentially stable if and only if, for any symmetric positive-definite matrix M, there exists a unique symmetric positive-definite matrix Y that satisfies (28).

$$YA + A^T Y = -M. \tag{28}$$

Proof: Consider a matrix Y

$$Y = \int_0^\infty e^{A^T t} M e^{At} dt. \tag{29}$$

Then, the system is exponentially stable if it satisfies two conditions: 1) Y is a unique solution of (28) and 2) Y is a symmetric positive-definite matrix.

Putting (29) into (28), then

$$\begin{aligned} YA + A^T Y &= \int_0^\infty e^{A^T t} M e^{At} A dt + \int_0^\infty A^T e^{A^T t} M e^{At} dt \\ &= \int_0^\infty \frac{d}{dt}\left(e^{A^T t} M e^{At}\right) dt \\ &= \left[e^{A^T t} M e^{At}\right]_0^\infty \end{aligned}$$

Since the A is Hurwitz matrix, e^{At} approaches to zero as $t \to \infty$. Hence, it can be concluded that (29) satisfies (28).

A Lyapunov candidate function is defined as:

$$V = x^T P x. \tag{30}$$

The control goal (16) will be achieved by $\dot{V} < 0$, showing that $\dot{V}$ is negative definite. Taking the derivative of V:

$$\begin{aligned} \dot{V} &= x^T (PA + A^T P) x \\ &= -x^T M x \leq 0 \end{aligned} \tag{31}$$

Here, M is symmetric positive definite. The stability condition is related to the negative dynamics of the Lyapunov function V and it can be achieved by taking $x = 0$. Then, the tracking error decays exponentially.

B. CLOSED-SYSTEM STABILITY

Theorem 3: If the tracking error is defined as (17) and the SMC controller is designed as (19), then the closed system with the model (15) is exponentially stable.

Proof: The closed-system stability is analyzed by designing the following Lyapunov candidate function:

$$V = z^T S z, \tag{32}$$

where

$$S = S^T > 0.$$

Then, the following is obtained by taking the derivative of V:

$$\begin{aligned} \mu V + \dot{V} &= \mu V + (z^T S)' z + z^T S \dot{z} \\ &= \mu V + \dot{z}^T S z + z^T S \dot{z} \\ &= \mu V + (Az + BGz)^T S z + z^T S (Az + BGz) \\ &= \mu V + z^T A^T S z + z^T G^T B^T S z + z^T S A z + z^T S B G z \\ &= \mu V + z^T \left(SA + A^T S + SBG + G^T B^T S \right) z \\ &= \mu z^T S z + z^T \xi z \\ &= z^T (\mu S + \xi) z \\ &= z^T (-M) z \end{aligned} \tag{33}$$

Here,

$$\xi = SA + A^T S + SBG + G^T B^T S.$$

To ensure $\mu V + \dot{V} \leq 0$, it is necessary that $\mu S + \xi < 0$, that is,

$$\mu S + SA + A^T S + SBG + G^T B^T S < 0. \tag{34}$$

Since A is Hurwitz, then (34) can be guaranteed. The left-hand side of (34) is linearized, as the G and P are unknown. Q is defined as SBG. Then, the following is obtained:

$$\mu S + A^T S + Q^T + SA + Q < 0. \tag{35}$$

In other words, for LMI (23), it is necessary to design S as symmetrical matrix and the derivative of V is negative definite if and only if, M is a positive-definite matrix.

Lemma 1: Let $f, V : [0, \infty) \in R$; then,

$$\dot{V} \leq -\mu V + f, \forall t \geq t_0 \geq 0$$

implies that

$$V(t) \leq e^{-\mu(t-t_0)} V(t_0) + \int_{t_0}^{t} e^{-\mu(t-\tau)} f(\tau) d\tau, \forall t \geq t_0 \geq 0$$

for any finite constant μ. As

$$\mu V + \dot{V} \leq 0,$$

According to Lemma 1,

$$V(t) \leq V(0) \exp(-\mu t).$$

This guarantees the convergence of the tracking error to zero exponentially as $V(t)$ approaches to zero when $t \to \infty$ and the closed-system stability is guaranteed.

Lemma 2: If the following differential inequality is satisfied:

$$\dot{V}(t) \leq -\varepsilon V^{\eta}(t), \quad \forall t \geq t_0 \geq 0, \ V(t_0) \geq 0$$

where

$$\varepsilon > 0, 0 < \eta < 1$$

implies that

$$V^{1-\eta}(t) \leq V^{1-\eta}(t_0) - \varepsilon(1-\eta)(t - t_0), \ t_f \geq t \geq t_0 \tag{36}$$

and

$$V(0) \equiv 0, \quad \forall t \geq t_f$$

Then,

$$t_f = t_0 + \frac{V^{1-\eta}(t_0)}{\varepsilon(1-\eta)} \tag{37}$$

This guarantees the convergence of V to zero in finite time t_f. It means that the tracking error (17) will be zero for $t_f \leq t \leq \infty$.

V. MODELING OF FSCS

This section explains the control mechanism for FSCs, which is responsible for the transfer of active power and the exchange of reactive power between the WECS and the grid. As previously discussed, FSCs comprise an MSC and a GSC. Exhaustive mathematical modeling and the detailed formulation of the control systems for the MSC and GSC are presented in the following subsections.

A. MODELING OF MSC CONTROL

An MSC controller generates the optimal switching signals for the MSC to track the reference signals provided by a maximum power point tracking controller, i.e., the speed, in this study. The main objective is to capture as much power as possible from the wind. The SPMSG stator-voltage dynamics in the SRF are described by (38), and they assist in the discussion of the MSC control scheme.

$$\left.\begin{aligned} v_{ds} &= R_s i_{ds} + L_s \frac{di_{ds}}{dt} - \omega_e L_s i_{qs} \\ v_{qs} &= R_s i_{qs} + L_s \frac{di_{qs}}{dt} + \omega_e \left(L_s i_{ds} + \psi_{PM} \right) \end{aligned}\right\}. \tag{38}$$

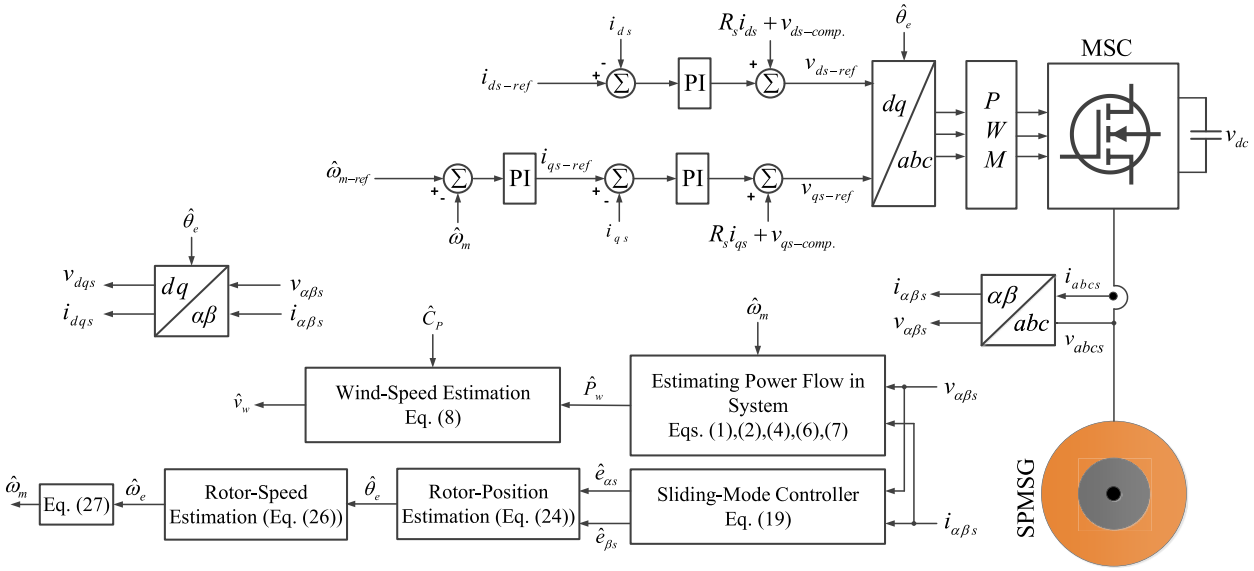

FIGURE 4. Schematic of the MSC control scheme.

The zero d-axis current control strategy is employed to provide the maximum electromagnetic torque (T_{em}), as the torque only depends on the q-axis component of the stator current [3]. It specifies that the generated power and stator q-axis current are virtually proportional. The stator q-axis current reference (i_{qs-ref}) is generated directly from the speed-control loop [36]. This loop employs a proportional-integral (PI) regulator in which the error between the rotor-speed reference and the estimated rotor speed is applied as an input. The mathematical expressions for stator-current references are as follows:

$$\left.\begin{aligned} i_{ds-ref} &= 0 \\ i_{qs-ref} &= PI\left(\hat{\omega}_{m-ref} - \hat{\omega}_m\right) \end{aligned}\right\}. \tag{39}$$

Figure 4 presents a schematic of an MSC control system. It comprises a dual-control loop structure having fast inner current-control loops and a slow outer speed-control loop.

The error signals of the stator dq currents produce stator dq voltages (40) through the corresponding PI controllers.

$$\left.\begin{aligned} v'_{ds} &= PI(i_{ds-ref} - i_{ds}) \\ v'_{qs} &= PI(i_{qs-ref} - i_{qs}) \end{aligned}\right\}. \tag{40}$$

To achieve decoupled current controls, feedforward compensation terms ($v_{ds-comp.}$ and $v_{qs-comp.}$) are added to the outputs of the current dq-axes PI controllers (40) to obtain stator dq voltage references:

$$\left.\begin{aligned} v_{ds-ref} &= v'_{ds} + v_{ds-comp.} + R_s i_{ds} \\ v_{qs-ref} &= v'_{qs} + v_{qs-comp.} + R_s i_{qs} \end{aligned}\right\}. \tag{41}$$

The compensation terms improve the dynamic response of the system and are described as follows:

$$\left.\begin{aligned} v_{ds-comp.} &= -\hat{\omega}_e L_s i_{qs} \\ v_{qs-comp.} &= \hat{\omega}_e L_s i_{ds} \end{aligned}\right\}. \tag{42}$$

Finally, the obtained stator-voltage references are applied to a pulse width modulation to produce switching signals for controlling the MSC.

B. MODELING OF GSC CONTROL

As mentioned previously, a GSC is primarily used to regulate the DC-link voltage for the MSC and to provide reactive-power support for the grid voltage. In this study, voltage-oriented vector control is employed to control the GSC for achieving decoupled control of the active and reactive powers between the GSC and the grid. The voltage dynamics for a GSC in the SRF can be expressed as follows:

$$\left.\begin{aligned} u_{dg} &= R_f i_{dg} + L_f \frac{d}{dt} i_{dg} - \omega_g L_f i_{qg} + v_{dg} \\ u_{qg} &= R_f i_{qg} + L_f \frac{d}{dt} i_{qg} + \omega_g L_f i_{dg} + v_{qg} \end{aligned}\right\}, \tag{43}$$

In (43), the subscript g denotes the grid-side quantities; u_{dg} and u_{qg} are the d and q components of the grid voltage, respectively; v_{dg} and v_{qg} represent the GSC voltage vectors in the dq frame, respectively. The active power and reactive power exchanged between the GSC and the grid are defined as follows:

$$\left.\begin{aligned} P_g &= 1.5\left(u_{dg} i_{dg} + u_{qg} i_{qg}\right) \\ Q_g &= 1.5\left(u_{qg} i_{dg} - u_{dg} i_{qg}\right) \end{aligned}\right\}. \tag{44}$$

The d-axis of the dq reference frame is aligned with the grid-voltage direction, whereas the q-axis rotates 90° along the d-axis shaft. Thus, the dq components of the grid-voltage vector are derived as follows:

$$\left.\begin{aligned} u_{dg} &\cong V_g \\ u_{qg} &= 0 \end{aligned}\right\} \tag{45}$$

In this context, (44) can be written as follows:

$$\left.\begin{aligned} P_g &= 1.5 u_{dg} i_{dg} \\ Q_g &= -1.5 u_{dg} i_{qg} \end{aligned}\right\} \tag{46}$$

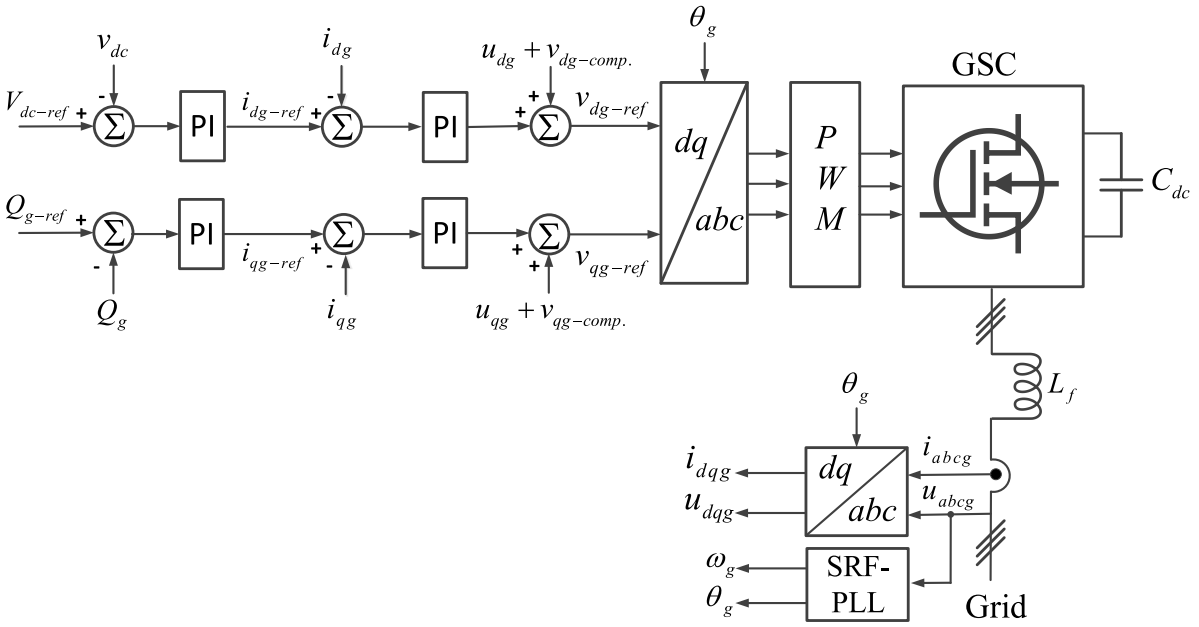

FIGURE 5. Schematic of the GSC control scheme.

Equation (46) describes the relationship between the active power and reactive power with i_{dg} and i_{qg}, considering the grid-voltage (u_{dg}) constant. The DC-side equation of the GSC is written as follows:

$$C_{dc}\frac{d}{dt}v_{dc} = \left(\frac{v_{dg}}{v_{dc}}i_{dg} + \frac{v_{qg}}{v_{dc}}i_{qg}\right) - i_{dc}. \tag{47}$$

Figure 5 presents a schematic of the GSC control, which comprises a cascaded control-loop structure. The fast inner current-control loops are used to regulate the d- and q-axis components of the grid-side current, whereas the slow outer-loop controllers are used to control the DC-link voltage and reactive power of the converter. The d-axis component of the grid-side current reference is generated by a PI controller after the reference and measured values of the DC-link voltage are compared. The error signal of the reference and actual reactive powers is fed to a PI controller to obtain the q-axis component of the grid-side current reference. Analytical expressions for the grid-side dq current references are given as follows:

$$\left.\begin{aligned} i_{dg-ref} &= PI\left(V_{dc-ref} - v_{dc}\right) \\ i_{qg-ref} &= PI\left(Q_{g-ref} - Q_g\right) \end{aligned}\right\}, \quad Q_{g-ref} = 0. \tag{48}$$

The d- and q-axis voltage references are generated by adding the feedforward terms $v_{dg-comp.}$ and $v_{qg-comp.}$, respectively, yielding

$$\left.\begin{aligned} v_{dg-ref} &= PI\left(i_{dg-ref} - i_{dg}\right) + v_{dg-comp.} + u_{dg} \\ v_{qg-ref} &= PI\left(i_{qg-ref} - i_{qg}\right) + v_{qg-comp.} + u_{qg} \end{aligned}\right\}. \tag{49}$$

The feedforward terms are as follows:

$$\left.\begin{aligned} v_{dg-comp.} &= -\omega_g L_f i_{qg} \\ v_{qg-comp.} &= \omega_g L_f i_{dg} \end{aligned}\right\} \tag{50}$$

The obtained dq voltage references are transformed into the three-phase stationary-reference-frame coordinate system for controlling the GSC.

VI. RESULTS AND DISCUSSIONS

This section aims to validate the performances of the proposed wind-speed and rotor-position/speed estimation schemes for a 250-kW SPMSG-based WT test system, as shown in Fig. 1. In support of the theoretical explanation and mathematical modeling of the proposed algorithms for wind-speed estimation and sensorless control for an SPMSG presented in Section III, extensive numerical simulations are performed in MATLAB/Simulink. The WT, SPMSG, and grid parameters are presented in Appendix A. Moreover, the proposed schemes are evaluated by defining two different scenarios to ensure that they would be capable of covering all the operational regimes of a WECS.

- Scenario 1: Constant and slowly varying wind-speed conditions
- Scenario 2: Suddenly and significantly varying wind-speed conditions

The obtained results verify the excellent steady-state and dynamic performances and good precision of the proposed solutions for sensorless control of an SPMSG and wind-speed estimation.

A. SCENARIO 1: CONSTANT AND SLOWLY VARYING WIND-SPEED CONDITIONS

In this subsection, constant and slowly varying wind-speed dynamics are discussed, and their impacts on the estimated values of the rotor position, rotor speed, and wind speed are examined. The behaviors of the proposed estimation algorithms are highlighted with the help of the obtained

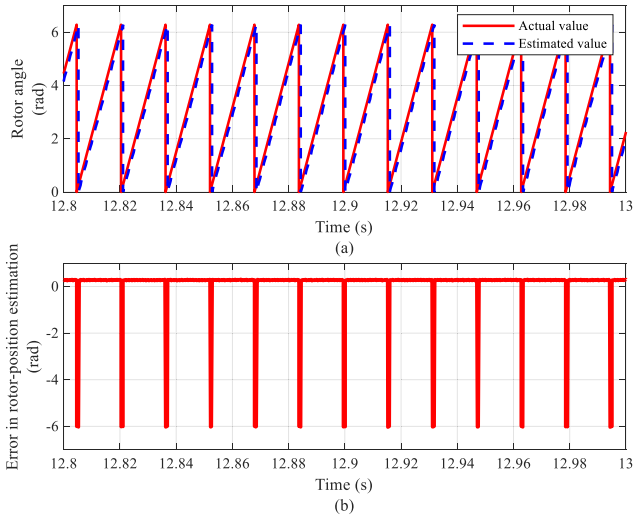

FIGURE 6. Simulation results for constant and slowly varying wind speeds: (a) rotor-position estimation and (b) error of estimated rotor position.

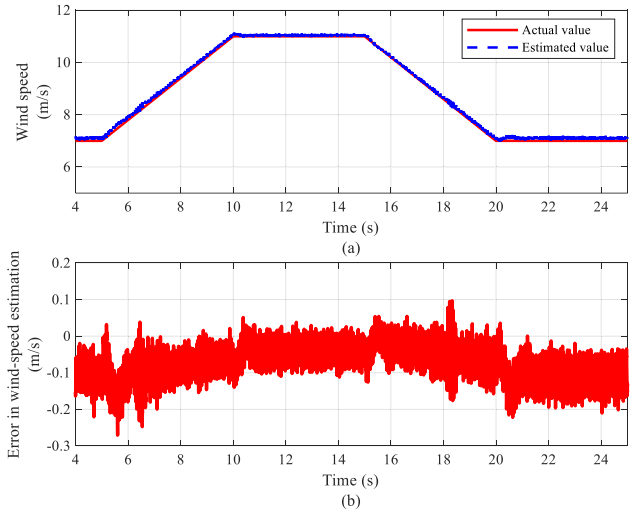

FIGURE 7. Simulation results for constant and slowly varying wind speeds: (a) wind-speed estimation and (b) error of estimated wind speed.

simulation results. The wind speed varies in the range of ± 4 m/s with a rate of ± 0.8 m/s and remains constant at 11 m/s from 10 to 15 s.

A modulus operation is used to ensure the changes in the rotor-position angle into the interval $[0,2\pi)$. The actual rotor position determined by the position sensor and the estimated value of the rotor position obtained via the proposed scheme are compared in Fig. 6(a), whereas Fig. 6(b) shows the corresponding error between the estimated and actual rotor angles. It is observed that the transient error occurs up to 2π radians whenever the actual rotor position resets its value from 2π to 0 radians, however, the error decays exponentially. This is due to a small difference between the estimated and actual rotor positions and becomes significant when the modulus operation triggers. The results confirm the accurate estimation of the rotor position using the proposed LMI-based SMC method.

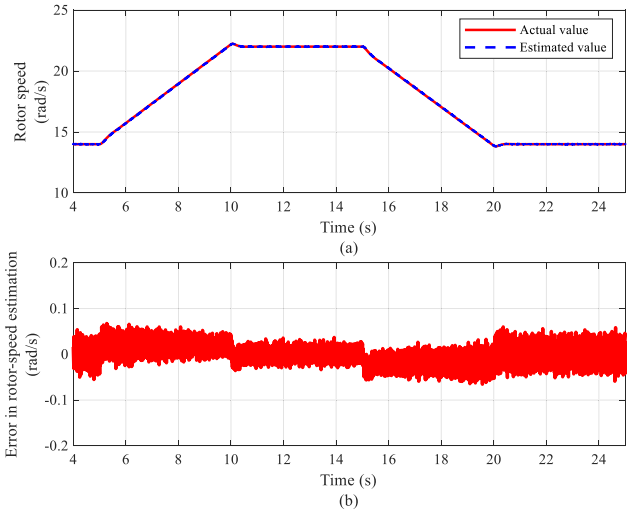

FIGURE 8. Simulation results for constant and slowly varying wind speeds: (a) rotor-speed estimation and (b) error of estimated rotor speed.

The simulation results for the actual and estimated wind speeds are presented in Fig. 7(a), and the error in the wind-speed estimation is shown in Fig. 7(b). With the application of the proposed technique, the estimated wind speed closely follows the actual wind speed, with slight variations, and no directionality problem is observed in the estimation.

Moreover, as shown in Fig. 8(a), the rotor speed is regulated well, following its actual value with good precision, after the proposed method is applied. The insignificant variations between the actual and estimated rotor speeds, as shown in Fig. 8(b), indicate the satisfactory performance of the proposed design.

It is worth mentioning that the actual and estimated values of the rotor position, wind speed, and rotor speed obtained using the proposed algorithms under constant and slowly varying wind-speed conditions are similar.

B. SCENARIO 2: SUDDENLY AND SIGNIFICANTLY VARYING WIND-SPEED CONDITIONS

This subsection focuses on highlighting the performance of the proposed estimation methods under sudden and large wind-speed variations. The same estimated parameters used in case of slowly varying wind-speed conditions are considered here. The wind speed suddenly increases from 11 to 14 m/s at 5 s and decreases to 9 m/s at 12 s. The speed remains constant up to 20 s and then abruptly increases to 11 m/s.

Figure 9(a)–(b) presents a comparison between the actual and estimated values of the rotor position and the corresponding error between them, respectively, in response to the aforementioned sudden changes in the wind speed. As expected, the same results are achieved here as those obtained in case of slowly varying wind-speed conditions. The results confirm the effectiveness of the proposed algorithms for tracking the actual rotor position accurately under sudden and large wind-speed changes.

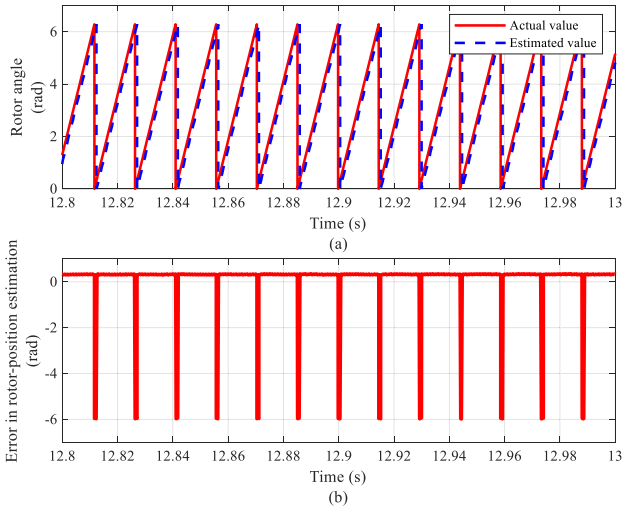

FIGURE 9. Simulation results for sudden and large wind-speed variations: (a) rotor-position estimation and (b) error of estimated rotor position.

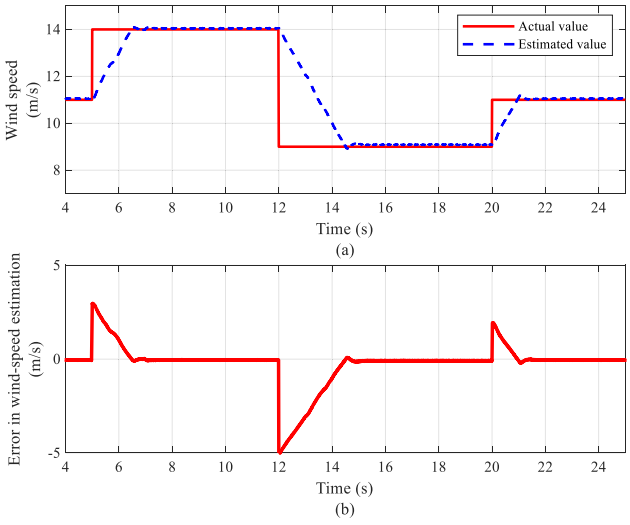

FIGURE 10. Simulation results for sudden and large wind-speed variations: (a) wind-speed estimation and (b) error of estimated wind speed.

The estimated wind speed attempts to track sudden changes in wind-speed conditions. However, it takes time to cater such large variations, as indicated in Fig. 10(a). Initially, a large transient error is observed whenever a sudden change occurs; however, the error decreases quickly, and the estimated wind speed ultimately follows the actual speed, as shown in Fig. 10(b).

Furthermore, the simulation results for the actual and estimated rotor speeds under the aforementioned conditions are presented in Fig. 11(a). Good agreement is observed between them, and the error in the rotor-speed estimation is shown in Fig. 11(b). As expected, when the proposed algorithms are employed, the estimated rotor speed closely follows its reference.

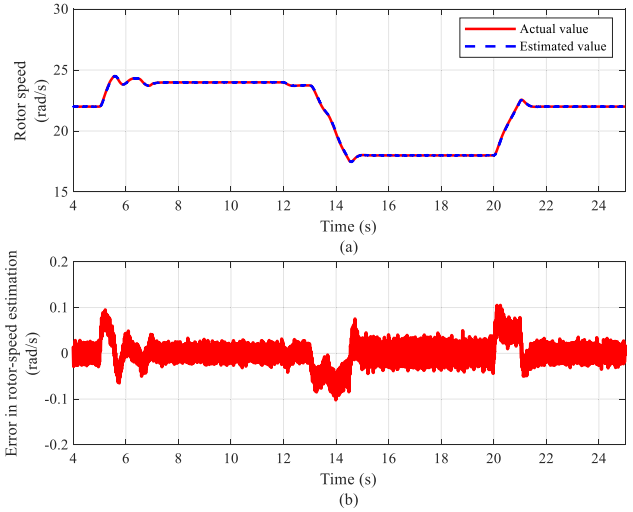

FIGURE 11. Simulation results for sudden and large wind-speed variations: (a) rotor-speed estimation and (b) error of estimated rotor speed.

The simulation results indicate that the proposed schemes are capable of estimating the wind speed, rotor position, and rotor speed accurately during sudden and large variations in the wind-speed conditions.

VII. CONCLUSION

Two estimation schemes for estimating and tracking the wind-speed and rotor-position/speed dynamics were designed and presented to achieve sensorless control for an SPMSG-based WECS. The following conclusions are drawn:

- A simple and effective wind-speed estimation method based on backpropagation nonlinear power dynamics was proposed and validated via simulations.
- A simple implementation of an SMC based on an LMI was achieved to track the actual rotor position and rotor speed of an SPMSG, making this scheme attractive.
- The effectiveness of the proposed LMI-based SMC design was confirmed and verified for challenging wind-speed conditions.
- The simulation results revealed that the estimation schemes had good tracking performance, with a high tracking precision and a fast response, indicating that they are promising for SPMSG-based WPSs.
- Satisfactory steady-state and dynamic performance of the proposed schemes was observed, with trivial tracking errors, in rotor-position/speed estimations.

Future studies may involve the experimental implementation and verification of the proposed schemes on a small test rig.

APPENDIX

The important parameters of the WT, SPMSG, and grid used in the simulated test system are presented in Tables 1, 2, and 3, respectively.

TABLE 1. Parameters of 250-kW WT.

Parameter	Value	Unit
Turbine rated power	250	kW
Rotor radius	14.8	m
Air density	1.225	kg/m^3
Maximum power coefficient	0.48	-
Optimal tip-speed ratio	8.1	-

TABLE 2. Parameters of 250-kW SPMSG.

Parameter	Value	Unit
Generator rated power	250	kW
Rated frequency	50	Hz
Stator resistance	0.04	Ω
Stator inductance	1.5	mH
Rotational inertia	100	kg.m^2
Pole-pair number	18	Nos.
Flux linkage	1.052	V·s
Viscous damping	2.5	N·m·s

TABLE 3. Parameters of grid-side components.

Parameter	Value	Unit
DC-link voltage reference	1200	V
DC-link capacitance	3.75	mF
Grid-side filter resistance	0.01	Ω
Grid-side filter inductance	0.8	mH
Rated grid voltage (phase-phase)	400	V(RMS)
Rated grid frequency	50	Hz

REFERENCES

[1] D. Jena and S. Rajendran, "A review of estimation of effective wind speed based control of wind turbines," *Renew. Sustain. Energy Rev.*, vol. 43, pp. 1046–1062, Mar. 2015.
[2] Y. Zhao, C. Wei, Z. Zhang, and W. Qiao, "A review on position/speed sensorless control for permanent-magnet synchronous machine-based wind energy conversion systems," *IEEE J. Emerg. Sel. Topics Power Electron.*, vol. 1, no. 4, pp. 203–216, Dec. 2013.
[3] M. A. S. Ali, K. K. Mehmood, and C.-H. Kim, "Full operational regimes for SPMSG-based WECS using generation of active current references," *Int. J. Electr. Power Energy Syst.*, vol. 112, pp. 428–441, Nov. 2019.
[4] M. Abdelrahem, C. M. Hackl, and R. Kennel, "Finite position set-phase locked loop for sensorless control of direct-driven permanent-magnet synchronous generators," *IEEE Trans. Power Electron.*, vol. 33, no. 4, pp. 3097–3105, Apr. 2018.
[5] W. Qiao, X. Yang, and X. Gong, "Wind speed and rotor position sensorless control for direct-drive PMG wind turbines," *IEEE Trans. Ind. Appl.*, vol. 48, no. 1, pp. 3–11, Jan. 2012.
[6] H. Li, K. Shi, and P. Mclaren, "Neural-network-based sensorless maximum wind energy capture with compensated power coefficient," *IEEE Trans. Ind. Appl.*, vol. 41, no. 6, pp. 1548–1556, Nov. 2005.
[7] W. Qiao, W. Zhou, J. Aller, and R. Harley, "Wind speed estimation based sensorless output maximization control for a wind turbine driving a DFIG," *IEEE Trans. Power Electron.*, vol. 23, no. 3, pp. 1156–1169, May 2008.
[8] K. Tan and S. Islam, "Optimum control strategies in energy conversion of PMSG wind turbine system without mechanical sensors," *IEEE Trans. Energy Convers.*, vol. 19, no. 2, pp. 392–399, Jun. 2004.
[9] A. Abo-Khalil and D.-C. Lee, "MPPT control of wind generation systems based on estimated wind speed using SVR," *IEEE Trans. Ind. Electron.*, vol. 55, no. 3, pp. 1489–1490, Mar. 2008.
[10] S. Wu, Y. Wang, and S. Cheng, "Extreme learning machine based wind speed estimation and sensorless control for wind turbine power generation system," *Neurocomputing*, vol. 102, pp. 163–175, Feb. 2013.
[11] B. Boukhezzar and H. Siguerdidjane, "Nonlinear control of a variable-speed wind turbine using a two-mass model," *IEEE Trans. Energy Convers.*, vol. 26, no. 1, pp. 149–162, Mar. 2011.
[12] F. D. Kanellos and N. D. Hatziargyriou, "Optimal control of variable speed wind turbines in islanded mode of operation," *IEEE Trans. Energy Convers.*, vol. 25, no. 4, pp. 1142–1151, Dec. 2010.
[13] Z. Xu, Q. Hu, and M. Ehsani, "Estimation of effective wind speed for fixed-speed wind turbines based on frequency domain data fusion," *IEEE Trans. Sustain. Energy*, vol. 3, no. 1, pp. 57–64, Jan. 2012.
[14] M. Mohandes, S. Rehman, and S. Rahman, "Estimation of wind speed profile using adaptive neuro-fuzzy inference system (ANFIS)," *Appl. Energy*, vol. 88, no. 11, pp. 4024–4032, Nov. 2011.
[15] S. Shamshirband, D. Petković, N. B. Anuar, M. L. M. Kiah, S. Akib, A. Gani, Ž. Ćojbašic, and V. Nikolić, "Sensorless estimation of wind speed by adaptive neuro-fuzzy methodology," *Int. J. Electr. Power Energy Syst.*, vol. 62, pp. 490–495, Nov. 2014.
[16] K. Mok, "Wind speed estimation algorithm in the presence of observation noise," *J. Sol. Energy Eng.*, vol. 132, no. 1, pp. 1–6, Dec. 2009.
[17] S. Morimoto, K. Kawamoto, M. Sanada, and Y. Takeda, "Sensorless control strategy for salient-pole PMSM based on extended EMF in rotating reference frame," *IEEE Trans. Ind. Appl.*, vol. 38, no. 4, pp. 1054–1061, Jul. 2002.
[18] K.-W. Hu and C.-M. Liaw, "Position sensorless surface-mounted permanent-magnet synchronous generator and its application to power DC microgrid," *IET Power Electron.*, vol. 8, no. 9, pp. 1636–1650, Sep. 2015.
[19] S. Chi, Z. Zhang, and L. Xu, "Sliding-mode sensorless control of direct-drive pm synchronous motors for washing machine applications," *IEEE Trans. Ind. Appl.*, vol. 45, no. 2, pp. 582–590, Mar./Apr. 2009.
[20] G. Foo and M. Rahman, "Sensorless sliding-mode MTPA control of an IPM synchronous motor drive using a sliding-mode observer and HF signal injection," *IEEE Trans. Ind. Electron.*, vol. 57, no. 4, pp. 1270–1278, Apr. 2010.
[21] Y. Zhao, W. Qiao, and L. Wu, "An adaptive quasi-sliding-mode rotor position observer-based sensorless control for interior permanent magnet synchronous machines," *IEEE Trans. Power Electron.*, vol. 28, no. 12, pp. 5618–5629, Dec. 2013.
[22] X. Song, J. Fang, B. Han, and S. Zheng, "Adaptive compensation method for high-speed surface PMSM sensorless drives of EMF-based position estimation error," *IEEE Trans. Power Electron.*, vol. 31, no. 2, pp. 1438–1449, Feb. 2016.
[23] G. Zhang, G. Wang, D. Xu, and N. Zhao, "ADALINE-network-based PLL for position sensorless interior permanent magnet synchronous motor drives," *IEEE Trans. Power Electron.*, vol. 31, no. 2, pp. 1450–1460, Feb. 2016.
[24] Z. Chen, J. Gao, F. Wang, Z. Ma, Z. Zhang, and R. Kennel, "Sensorless control for SPMSM with concentrated windings using multisignal injection method," *IEEE Trans. Ind. Electron.*, vol. 61, no. 12, pp. 6624–6634, Dec. 2014.
[25] M. N. Uddin and N. Patel, "Maximum power point tracking control of IPMSG incorporating loss minimization and speed sensorless schemes for wind energy system," *IEEE Trans. Ind. Appl.*, vol. 52, no. 2, pp. 1902–1912, Mar./Apr. 2016.
[26] J. Yang, W. Tang, G. Zhang, Y. Sun, S. Ademi, F. Blaabjerg, and Q. Zhu, "Sensorless control of brushless doubly fed induction machine using a control winding current MRAS observer," *IEEE Trans. Ind. Electron.*, vol. 66, no. 1, pp. 728–738, Jan. 2019.
[27] M. Kumar, S. Das, and K. Kiran, "Sensorless speed estimation of brushless doubly-fed reluctance generator using active power based MRAS," *IEEE Trans. Power Electron.*, vol. 34, no. 8, pp. 7878–7886, Aug. 2019.
[28] J. M. Guerrero, C. Lumbreras, D. Reigosa, D. Fernandez, F. Briz, and C. B. Charro, "Accurate rotor speed estimation for low-power wind turbines," *IEEE Trans. Power Electron.*, vol. 35, no. 1, pp. 373–381, Jan. 2020.
[29] J. Hui, A. Bakhshai, and P. Jain, "An energy management scheme with power limit capability and an adaptive maximum power point tracking for small standalone PMSG wind energy systems," *IEEE Trans. Power Electron.*, vol. 31, no. 7, pp. 4861–4875, Jul. 2016.
[30] J. M. Guerrero, C. Lumbreras, D. D. Reigosa, P. Garcia, and F. Briz, "Control and emulation of small wind turbines using torque estimators," *IEEE Trans. Ind. Appl.*, vol. 53, no. 5, pp. 4863–4876, Sep. 2017.
[31] C. Lumbreras, J. M. Guerrero, P. Garcia, F. Briz, and D. D. Reigosa, "Control of a small wind turbine in the high wind speed region," *IEEE Trans. Power Electron.*, vol. 31, no. 10, pp. 6980–6991, Oct. 2016.

[32] A. Hebala, W. A. M. Ghoneim, and H. A. Ashour, "Detailed design procedures for PMSG direct-driven by wind turbines," *J. Electr. Eng. Technol.*, vol. 14, no. 1, pp. 251–263, Jan. 2019.
[33] S. J. Chapman, *Electric Machinery Fundamental Applications*, 4th ed. New York, NY, USA: McGraw-Hill, 2005, pp. 261–262.
[34] M. A. S. Ali, K. K. Mehmood, J. S. Kim, and C.-H. Kim, "ESD-based crowbar for mitigating DC-link variations in a DFIG-based WECS," in *Proc. IPST*, Perpignan, France, 2019, pp. 1–6.
[35] J. Chen, T. Lin, C. Wen, and Y. Song, "Design of a unified power controller for variable-speed fixed-pitch wind energy conversion system," *IEEE Trans. Ind. Electron.*, vol. 63, no. 8, pp. 4899–4908, Aug. 2016.
[36] G. Abad, *Power Electronics and Electric Drives for Traction Applications*. Hoboken, NJ, USA: Wiley, 2017, pp. 104–105, and 124–125.

MUHAMMAD ARIF SHARAFAT ALI received the B.Sc. degree in electrical engineering from the University of Engineering and Technology Lahore, Pakistan, in 2002, and the M.S. degree in energy systems engineering from Sungkyunkwan University, South Korea, in 2017, where he is currently pursuing the Ph.D. degree in electrical and computer engineering. His research interests include grid integration of wind-power plants, control of wind-energy conversion systems, and power system dynamic and control.

KHAWAJA KHALID MEHMOOD received the B.Sc. and Ph.D. degrees in electrical power engineering from the Mirpur University of Science and Technology, Mirpur, Pakistan, and Sungkyunkwan University, South Korea, in 2012 and 2019, respectively. He is currently working as an Assistant Professor with the U.S.-Pakistan Centre for Advanced Studies in Energy (USPCAS-E), National University of Sciences and Technology, Islamabad, Pakistan. His research interests include planning and operations of active distribution systems, machine learning applications in distribution systems, electric vehicles, and battery energy storage systems.

SHAZIA BALOCH received the B.Sc. degree in electrical engineering from the Balochistan University of Engineering and Technology, Khuzdar, Pakistan, in 2010, and the M.S. degree in electrical power engineering from the Mehran University of Engineering and Technology, Jamshoro, Pakistan, in 2016. She is currently pursuing the Ph.D. degree in electrical and computer engineering with Sungkyunkwan University, South Korea. Her research interests include power electronics and microgrid protection.

CHUL-HWAN KIM (Senior Member, IEEE) received the B.S., M.S., and Ph.D. degrees in electrical engineering from Sungkyunkwan University, South Korea, in 1982, 1984, and 1990, respectively.

In 1990, he joined Cheju National University, Cheju, South Korea, as a Full-Time Lecturer. He was a Visiting Academic with the University of Bath, Bath, U.K., in 1996, 1998, and 1999, respectively. He has been a Professor with the College of Information and Computer Engineering, Sungkyunkwan University, since 1992, where he is currently the Director of the Center for Power Information Technology. His current research interests include power system protection, artificial intelligence applications for protection and control, modeling/protection of underground cable, and electromagnetic transients program software.